Color Changes Caused by Conformational Polymorphism: Optical-Crystallography, Single-Crystal Spectroscopy, and Computational Chemistry

Lian Yu*

Lilly Research Laboratories, Eli Lilly and Company, Indianapolis, Indiana 46285

Received: August 6, 2001; In Final Form: November 1, 2001

5-Methyl-2-[(2-nitrophenyl)amino]-3-thiophenecarbonitrile (**1**) crystallizes as seven conformational polymorphs of red, orange, and yellow colors. Comparable thermodynamic stability of the polymorphs enables the solution of six crystal structures, a number unmatched by current entries in the Cambridge Structural Database, making **1** well suited for structure−property studies. The different crystal colors of **1** have been studied using optical crystallography, polarized single-crystal absorption spectroscopy and computational methods. Different crystal colors ("color polymorphism") are well explained by the conformational differences between polymorphs, which cause varying degrees of π-conjugation between the *o*-nitroaniline chromophore and the thiophene group. The isolation of different conformers in crystal polymorphs permits an evaluation of computational models of electronic structures and transitions through observed spectral properties. The newly matured Time Dependent Density Functional Theory gave the best reproduction of observed wavelengths, oscillator strengths, and directions of electronic transition dipole moments, outperforming Configuration Interaction Singles, and even ZINDO, a semiempirical model specially calibrated on electronic spectra.

Introduction

Polymorphism, the ability of a molecule to adopt different crystal structures, provides special challenges and opportunities to chemical research and development. The manufacturers of drugs,[1,2] lipids,[3] pigments, explosives, and other specialty chemicals must characterize and control polymorphism to avoid changes in product properties, variability of crystallization outcome, and unexpected disappearance of polymorphs.[4] Polymorphism is useful for the study of structure−property relationships in molecular solids[5−9] because property differences between polymorphs stem only from different molecular packing and/or conformation and not from different chemical compositions. The polymorphism arising from chiral molecules enables one to study whether a special affinity exists between molecules of opposite chirality that causes racemic solutions to crystallize predominantly as racemic compounds rather than conglomerates.[10,11] The poor thermodynamic selectivity of polymorphic crystallization, frequently observed owing to the small free-energy difference between polymorphs (ca. 1 kJ/mol),[12] motivates the development of kinetic strategies for selective nucleation.[13−15]

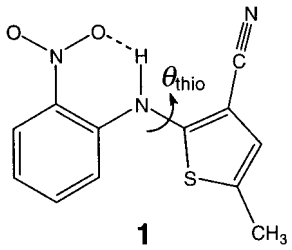

1

Polymorphism-based studies are augmented by systems possessing numerous, diverse and known crystal structures. This feature is found in 5-methyl-2-[(2-nitrophenyl)amino]-3-thiophenecarbonitrile (**1**), which crystallizes in at least seven solvent-free polymorphs. Among these, six crystal structures have been solved (Table 1),[7,16] making the system not only one of the most polymorphic, but also one having the most members for which single-crystal structures are solved in the current Cambridge Structural Database.[17,18] Other remarkable features of **1** include conformational polymorphism[19] and different crystal colors (red, orange, and yellow). Conformational polymorphism refers to the adoption of different molecular conformations in different polymorphs. In the case of **1**, the conformational difference is most pronounced in the torsional angle θ_{thio} (Table 1).

A previous study of **1**[7] examined how thermodynamic stability is influenced by crystal structure. Yu et al. demonstrated that although perpendicular conformers ($\theta_{thio} \approx \pm 90°$) are preferred in solution and gas phase, lower-energy crystals are built by conformers that are more coplanar ($\theta_{thio} \approx 0°$) and have higher dipole moments. The same preference prevails among other Ar_1-Ar_2 type molecules, where Ar_1 and Ar_2 are rigid aromatic rings connected by a single bond.[20−22]

A second study of **1**[15] investigated the poor polymorphic selectivity of crystallization and whether selective nucleation could be achieved with the aid of single-crystal substrates. Mitchell et al. demonstrated that the (101) face of pimelic acid selectively nucleates a metastable polymorph (YN) through optimal epitaxial match. The same study also showed that the (010) face of succinic acid, though less selective as a nucleation template, leads to oriented growth of a previously unknown polymorph, the seventh in the family.

The present study returned to structure−property relationships, focusing on the structural origin of red, orange, and yellow colors of the polymorphs. Of interest here were two related questions: Are different crystal colors explainable by conformational differences between polymorphs? Can observed conformation−color relationships be used to test theories of electronic structures and transitions? Thin crystals suitable for

* To whom correspondence ahould be addressed. Tel.: (317) 276-1448. Fax: (317) 277-2154. E-mail: yu_lian@lilly.com.

10.1021/jp013019c CCC: $22.00
Published on Web 12/28/2001

TABLE 1: Crystal Data for the Polymorphs of 1

form	Y	YN	ON	OP	ORP	R
system	monoclinic	triclinic	monoclinic	monoclinic	orthorhombic	triclinic
spc grp [No.]	$P2_1/n$ [14]	$P\bar{1}$ [2]	$P2_1/c$ [14]	$P2_1/n$ [14]	*Pbca* [61]	$P\bar{1}$[2]
color	yellow	yellow	orange	orange	orange-red	red
habit	prism	needle	needle	plate	plate	prism
a, Å	8.5001(8)	4.5918(8)	3.9453(7)	7.9760(9)	13.177(3)	7.4918(5)
b, Å	16.413(2)	11.249(2)	18.685(1)	13.319(2)	8.0209(18)	7.7902(5)
c, Å	8.5371(5)	12.315(2)	16.3948(4)	11.676(1)	22.801(5)	11.9110(8)
α, °	90	71.194(3)	90	90	90	75.494(6)
β, °	91.767(7)	89.852(4)	93.830(5)	104.683(8)	90	77.806(6)
γ, °	90	88.174(3)	90	90	90	63.617(6)
Z	4	2	4	4	8	2
θ_{thio}, °	104.7(2)	104.1(3)	52.6(4)	46.1(4)	39.4(5)	21.7(3)

absorption spectroscopy were grown and indexed by optical-crystallographic methods. Observed electronic spectra were compared with results of several computational methods: ZINDO, a semiempirical configuration-interaction method calibrated on electronic spectra;[23] Configuration Interaction-Singles (CIS), an ab initio approach based on configuration interaction among singly substituted determinants;[24] and the Time-Dependent Density Functional Theory (TD-DFT), a recently matured method for calculating electronic transitions.[25,26] The polymorphism of **1** is well suited for this purpose because different conformers, both stable and unstable in solution, are isolated in the six polymorphs of known structures. Owing to lattice rigidity, these otherwise flexible conformers undergo only vertical electronic transitions (i.e., transitions without conformational change), which simplifies theoretical analysis. In addition, single-crystal spectroscopy directly yields the direction of electronic transition dipole moment (ETDM), a property sensitive to the conformational effect on electronic structure and the quality of theoretical models.

Experimental Section

Crystallization. Crystal sections Y(010), ON(011), and R(111) were grown from benzyl alcohol solutions or a supercooled melt at room temperature between a microscope slide and a cover glass. The polymorphs were usually identifiable on sight from their colors and morphologies and when necessary, confirmed by Raman microscopy (Renishaw System 1000) or melting point (Linkam THMS 600 microscope hot-stage). Under the same condition, Form YN grew as fine-grained spherulites from the supercooled melt or curved thin needles from solution, neither being suitable for single-crystal spectroscopy. Polycrystalline spectra of YN were recorded through melt-grown spherulites. Thin plates of OP with well-developed $(10\bar{1})$ faces were obtained by room-temperature seeding of an ethylene glycol solution saturated at 60 °C. The first-generation seeds of OP were obtained unexpectedly when Form R was heated at 90 °C for 3 days. Solution grown OP crystals always coexisted with ON (orange needles) and were isolated manually and transferred to a microscope slide for observation. The simultaneous crystallization of multiple polymorphs ("concomitant polymorphism"[27]) was more prevalent in a supercooled melt, yielding as many as three or four polymorphs.

Optical Crystallography. Orthoscopic and conoscopic observations[28] were made with a Nikon Optiphot 2-Pol polarized light microscope. Profile angles (angles between the edges outlining a thin crystal section) were measured with a rotating stage (graduated to 1°; vernier readings to 6′). Conoscopic interference figures (CIFs) were observed through a 60× CF P Plan objective (n.a. = 0.85) and 20 nm-bandwidth interference filters (400 to 650 nm). Optic signs were determined using a quartz wedge.

Spectroscopy. Polarized single-crystal visible absorption spectroscopy was performed with an Instrument SA Raman microscope (Mole 3000) consisting of an Olympus BH-2 light microscope coupled to a two-stage monochromator [an ISA DHR 320 (600 lines/mm) followed by an ISA HR 640 (1200 lines/mm)]. The microscope was Koeller-illuminated with a 12 V, 100 W tungsten halogen source polarized by a dichroic polarizer (Melles−Griot). The beam size was set by the field-aperture to 100 μm, significantly smaller than the single-crystalline regions used (at least 200−400 μm wide). The substage aperture was set to n.a. = 0.1 to yield quasi-normal incidence (incidence angle = 5.7°). A Zeiss Neofluar Epiplan Pol 10× objective (n.a. = 0.3) was chosen for spectroscopy for its better near-UV transmission. The monochromator had a thermoelectrically cooled PMT detector (RCA C31034), and its calibration was checked against He−Ne laser and holmium glass.

A second dichroic polarizer was placed just before the entrance slit of the monochromator in parallel with the first polarizer in order to suppress the effect of extinction dispersion (wavelength dependence of crystal extinction directions between crossed polars). The following analysis demonstrates this idea. Let T_1 and T_2 be the crystal transmittance when the electric vector $\boldsymbol{E}$ is aligned in parallel to the privileged vibration directions of the crystal $\boldsymbol{n_1}$ and $\boldsymbol{n_2}$, respectively. A slight misalignment between $\boldsymbol{E}$ and $\boldsymbol{n_1}$ leads to a composite spectrum, with the new T_1 given by $[\cos^2\theta\ T_1 + \sin^2\theta\ T_2 + 2\sin\theta\cos\theta\ (T_1T_2)^{1/2}\cos\Delta]$, where θ is the degree of misalignment, Δ is the retardation introduced by the crystal between the $\boldsymbol{n_1}$- and $\boldsymbol{n_2}$-polarized lights. That is, the T_1 spectrum is "contaminated" by the T_2 and $(T_1T_2)^{1/2}\cos\Delta$ spectra, which amounts to 2% and 26%, respectively, at $\theta = 10°$. With the addition of a second polarizer, the observed T_1 becomes $[\cos^4\theta\ T_1 + \sin^4\theta\ T_2 + 2\sin^2\theta\cos^2\theta\ (T_1T_2)^{1/2}\cos\Delta]$. At $\theta = 10°$, the degree of "contamination" becomes 0.1% and 6%, respectively.

Whenever possible, solution-grown crystals were used for spectroscopic measurement. Melt-grown crystals were occasionally chosen because they could be grown thinner. With melt-grown crystals, the polymorphic identity and crystal orientation were carefully checked by Raman microscopy and conoscopic observations. Crystals were immersed in glycerol (nonsolvent) to minimize reflection loss. Polarized absorption spectra were recorded in the maximal and minimal absorption directions, Amax and Amin, and normalized against the background spectrum recorded with the crystal removed from the light path. All measurements were made at 22 °C without correction for reflection.

This study characterized the crystal colors of **1** by absorption rather than reflection spectroscopy. The modest extinction coefficient of **1** ($\log \epsilon = 3.7$ for the visible CT band) allowed the preparation of crystal sections that were thin enough (ca.

0.6 μm as estimated using Beer's law) for absorption spectroscopy without severe saturation. The chief advantage of absorption spectroscopy is the ease of sample preparation and the possibility of performing both optical-crystallographic and spectroscopic measurements with the same preparation. Reflection spectroscopy, though immune from spectral saturation, requires free-standing crystals with well-developed facets. Such crystals were difficult to obtain for a large number of polymorphs of **1** that were needed for structure-spectrum correlation. This difficulty arose from the preferential growth of thermodynamically more stable polymorphs and polymorphic conversions in slow crystallization.

A Beckman DU7500 spectrometer was used to record UV−vis absorption spectra of solutions (ca. 10^{-5} M in cyclohexane or methanol) and of the supercooled melt. The sample of supercooled melt was prepared between two quartz slides.

Computational Chemistry. Vertical electronic transitions were calculated by CIS,[23] TD-DFT,[25] and ZINDO,[23] all implemented in the Gaussian98 suite of programs,[29] with crystallographically determined coordinates[7] whose hydrogen positions have been re-optimized at the HF/6-31G(D) level. The lowest-energy conformation of **1** was obtained by energy minimization at the HF/6-31G(D) level. The structure of *o*-nitroaniline (ONA) was obtained by energy minimization at the CIS/6-31G(D) level. All molecular orbitals were used in ZINDO for configuration interaction. The DFT used was the B3LYP implementation.[30] The basis set 6-311+G(2D,P) was used for CIS and TD-DFT calculations; 3-21G(D), 6-31G(D), and 6-31+G(D) were also used to evaluate how computational results depend on basis sets. With reference to the visible spectrum of ONA, the chromophore of **1**, the CIS and TD-DFT results improved with increasing size and diffusiveness of the basis set. Among the basis sets tested, the largest performance improvement followed the inclusion of diffuse functions, i.e., from 6-31G(D) to 6-31+G(D), which is sensible given the charge-transfer nature of the electronic transition. The final choice of the basis set reflected the adequate convergence of computational results and the large resource demand for molecules the size of **1**.

Results and Discussion

Crystallization and Optical-Crystallography. Figure 1 shows the four single-crystal sections prepared for absorption spectroscopy, namely Y(010), OP(10$\bar{1}$), ON(011), and R(111), along with the appropriate molecular projections through them. The absorption spectrum of YN was obtained through a polycrystalline sample of YN. These five polymorphs cover the entire range of colors and conformations observed. Polymorphs ORP and RPL were not obtained under the conditions used, despite an extensive search using different solvents and temperatures. ORP crystals produced from normal solution crystallization were too thick for absorption spectroscopy. To date, Form RPL has been obtained only as 10 μm-sized sublimation deposits on the (010) plane of succinic acid,[15] a preparation unsuitable for this study.

Figure 1 shows only one of the two inversion-related faces for each crystal section [e.g., Y(010) but not Y(0$\bar{1}$0)], even though both were observed with equal probability. Inversion-related faces were distinguishable through the microscope by the way the crystal inclined relative to Amin and Amax directions, either as depicted in Figure 1 or as in the mirror image of Figure 1. Inversion-related faces being equivalent for absorption spectroscopy, only those in Figure 1 will be referred to hereafter.

The Miller indices (*hkl*) of each crystal section in Figure 1 were determined principally by matching observed and calculated profile angles (Table 2). Other optical-crystallographic observations that aided the assignment of Miller indices or the interpretation of crystal spectra are summarized below:

(*i*) The Y(010) section showed centered CIF with cross dispersion (optic sign = +), indicating it is normal to the monoclinic *b* axis. Y(010) was found to be the *yz* section of the refractive-index ellipsoid.[31]

(*ii*) The OP(10$\bar{1}$) section showed parallel and symmetric extinction and displaced optic axis figures (optic sign = −), indicating the monoclinic *b* axis is perpendicular to the optic axis plane (OAP).

(*iii*) The ON(011) section was elongated along the *a* axis. The oblique extinction, extinction dispersion and off-centered CIF (optic sign = +) ruled out (001) and (010) as possible indices.

(*iv*) The R(111) sections were identified only by profile angles, since the triclinic symmetry imposes no symmetry requirement between crystallographic and principal axes. The CIF contained an off-centered optic axis with strong wavelength dependence (optic sign = −).

(*v*) Y(010), ON(011), and R(111) showed strong dichroism (different colors in polarized light at the two extinction directions), whereas OP(10$\bar{1}$) did not. This difference correlates with how the ETDMs are projected through the crystal sections (see later).

(*vi*) Y(010), ON(011), and R(111) showed extinction dispersion (wavelength dependence of the extinction directions between crossed polarizers), whereas OP(10$\bar{1}$) did not. The degree of extinction dispersion is shown in Figure 2. The lack of extinction dispersion for OP(10$\bar{1}$) is required by the monoclinic symmetry, since (10$\bar{1}$) is parallel to the *b* axis.

Solution and Melt Spectra. Figure 3 shows the solution and melt spectra of **1** and the solution spectrum of *o*-nitroaniline (ONA), the visible chromophore of **1**. The visible absorption of ONA arises from an in-plane charge transfer (CT) from the amino group to the nitro group, giving rise to its yellow color.[32] The CT bands of ONA and **1** overlap well at the blue edges, but differ significantly at the red edges, with the spectrum of **1** extending more into longer wavelengths, as indicated by the double-sided arrow. This difference is attributed to the existence of different conformers of **1** in solution, with the dominant perpendicular conformers ($\theta_{thio} \approx \pm 90°$) causing the absorption maximum and the more coplanar conformers (θ_{thio} approaching 0° or 180°) causing the red-shifted absorption. The same conclusion was reached previously via vibration spectroscopy and computational chemistry.[7] The CN stretch band of **1** in solution, reproduced above the visible spectra in Figure 3, shows a red-shifted shoulder, which was attributed to the more coplanar conformers in minor population. RHF/6-31G* calculations revealed a W-shaped potential-energy curve along θ_{thio} with minima at $\theta_{thio} = \pm 88.4°$ and maxima at $\theta_{thio} = 0°$ (+7.3 kJ/mol) and 180° (+15.3 kJ/mol). The shallowness of this potential energy curve should allow the population of higher energy, more coplanar conformers at room temperature.

The CT band of **1** in a supercooled melt ($\lambda_{max} = 410$ nm) is broader and more red-shifted than the solution counterpart, a feature that also finds a parallel in the IR CN spectrum. These features are explained by a higher concentration of the low θ_{thio} and high dipole conformers in the melt and the red-shift of CT bands in a polar medium.[32] Because the dipole moment of **1** increases from 4 to 8 D as θ_{thio} changes from 180° to 0°,[7] the

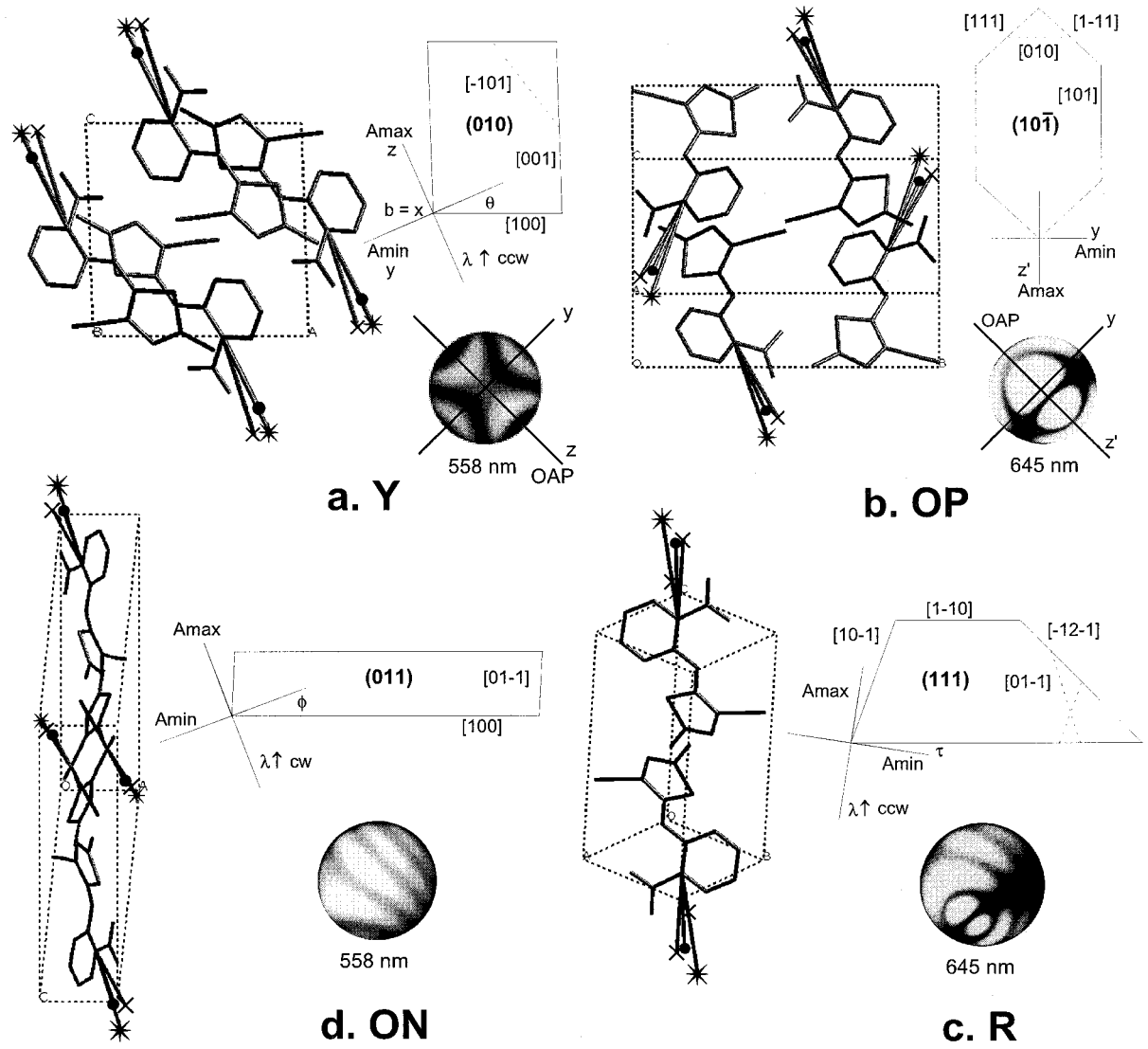

Figure 1. Morphologies, conoscopic interference figures (CIFs), Miller indices and molecular projections of single-crystal sections used for absorption spectroscopy: (a) Y(010); (b) OP(10$\bar{1}$); (c) ON(011); (d) R(111). By protocol, CIFs are shown at the 45° position, not the orientations at which crystals are drawn. Dotted lines in morphology drawings indicate alternative profile angles observed. Amin and Amax are directions of minimal and maximal absorption of plane-polarized light at the maximal absorption wavelength λ_{max}. $\lambda\uparrow$ cw and $\lambda\uparrow$ ccw indicate whether Amin and Amax rotate clockwise or counterclockwise with increasing wavelength relative to the crystal. The degrees of Amin and Amax rotation (extinction dispersion) are characterized by angles θ, ϕ and τ and shown in Figure 2. Calculated electronic transition dipole moments (ETDM) in debye are embedded in the molecular models of crystals as "bonds" starting at the phenyl carbon connecting to the nitro group and ending with symbols signifying computational methods: × for ZINDO, ● for TD-DFT, and ∗ for CIS. ZINDO returned two transitions for Form R: 419 nm ($f = 0.16$) and 453 nm ($f = 0.03$).

TABLE 2: Observed and Calculated Crystal Profile Angles (degree)

angle	obs.	calc.	angle	obs.	calc.
Y(010)			R(111)		
[100]^[001]	91.8	91.76	[01$\bar{1}$]^[$\bar{1}$2$\bar{1}$]	152.7	152.76
[100]^[00$\bar{1}$]	88.2	88.24	[01$\bar{1}$]^[12$\bar{1}$]	27.6	27.24
[001]^[$\bar{1}$01]	136.0	136.01	[10$\bar{1}$]^[0$\bar{1}$1]	142.8	142.64
[100]^[$\bar{1}$01]	135.8	135.76	[10$\bar{1}$]^[01$\bar{1}$]	37.4	37.36
OP(10$\bar{1}$)			[$\bar{1}$01]^[12$\bar{1}$]	64.6	64.60
[111]^[1$\bar{1}$1]	94.3	94.62	[$\bar{1}$01]^[$\bar{1}$2$\bar{1}$]	115.8	115.40
[101]^[111]	132.8	132.60	[1$\bar{1}$0]^[10$\bar{1}$]	109.7	109.81
ON(011)			[1$\bar{1}$0]^[10$\bar{1}$]	70.5	70.19
[$\bar{1}$00]^[011]	87.4	87.48	[1$\bar{1}$0]^[0$\bar{1}$1]	107.4	107.55
[$\bar{1}$00]^[011]	92.7	92.52	[1$\bar{1}$0]^[$\bar{1}$2$\bar{1}$]	134.8	134.79

low θ_{thio} conformers can be stabilized in the melt owing to favorable dipole−dipole interactions or equivalently, a reduction of the torsional barrier at $\theta_{thio} = 0°$.

Crystal Spectroscopy. Figure 4 shows the visible absorption spectra of the crystal sections in Figure 1 and a polycrystalline section of YN. By tracing the onset or maximum of the absorption peaks, one observes a progressive red-shift in the order Y ≈ YN < ON < OP < R, a trend in agreement with the visual inspection of crystal colors. The flattened top of the OP-(10$\bar{1}$) Amax spectrum indicates spectral saturation which was caused by the thickness of the crystal section used. Despite the slight spectral saturation, λ_{max} and λ_{onset} of OP(10$\bar{1}$) could be estimated with reasonable accuracy. For crystal sections showing extinction dispersion, the Amin and Amax directions were measured at λ_{max} as indicated by the open circles in Figure 2.

Computational Results. Table 3 shows the transition wavelengths λ_{max} and oscillator strengths f calculated by ZINDO, CIS/6-311+G(2D,P), and TD-DFT/6-311+G(2D,P). The visible CT band of ONA ($\lambda_{max} = 377$ nm and $f = 0.11$) was best reproduced by TD-DFT [$\Delta\lambda_{max} = (\lambda_{max\ calc} - \lambda_{max\ obs}) = -3$

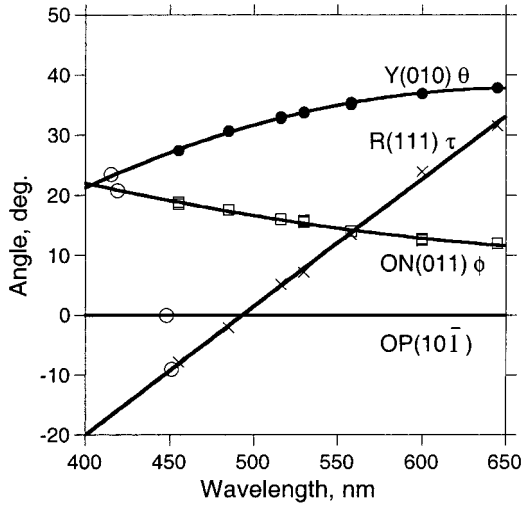

Figure 2. Extinction dispersion of the crystal sections in Figure 1, where the angles θ, τ, and ϕ are defined. The open circles indicate λ_{max}.

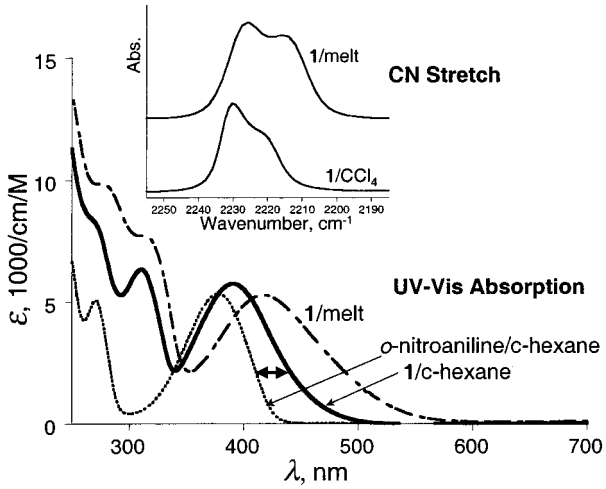

Figure 3. Bottom: UV−vis spectra of **1** in cyclohexane and its melt and the spectrum of *o*-nitroaniline (ONA), the visible chromophore of **1**, in cyclohexane. The visible band of ONA: $\lambda_{max} = 378$ nm, oscillator strength $f = 0.11$, dipole length $Q = 0.6$ Å. The visible band of **1**: $\lambda_{max} = 390$ nm, $f = 0.13$ and $Q = 0.7$ Å. Top: IR CN stretch bands of **1** in CCl_4 and its melt.

nm; $\Delta f = (f_{calc} - f_{obs})/f_{obs} \times 100\% = -18\%$], followed by ZINDO ($\Delta\lambda_{max} = +11$ nm and $\Delta f = +73\%$), and then by CIS ($\Delta\lambda_{max} = -125$ nm and $\Delta f = +130\%$). For the solution spectrum of **1**, the λ_{max} comparison is less meaningful since multiple conformers coexist in solution, each having different λ_{max}. The f comparison is more meaningful because f depends less strongly on conformation.[32] The f comparison gives the same ranking of performance: TD-DFT ($\Delta f = 0\%$), ZINDO ($\Delta f = +54\%$) and CIS ($\Delta f = +150\%$).

For the five crystal spectra in Figure 4, the average $\Delta\lambda_{max}$ is −19 nm for TD-DFT, −20 nm for ZINDO, and −179 nm for CIS.[33] Because ZINDO returned *two* visible transitions for the molecules of Form R (419 nm with $f = 0.16$ and 453 nm with $f = 0.03$), the average λ_{max} weighted by f was used in the calculation of $\Delta\lambda_{max}$. The crystal environment should cause a red-shift of the CT band of **1**, similar to its red-shift in polar solvents (+7 nm for **1** and +22 nm for ONA from cyclohexane to methanol). Given the large dipole moments of **1** in crystals (6−8 D depending on conformation[7]), the crystal red-shift is expected to be significant. An estimate of the crystal red-shift is +20 nm, the difference between the λ_{max} of the cyclohexane

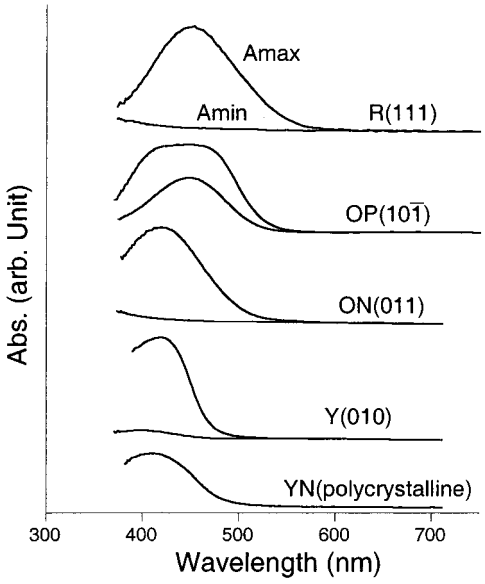

Figure 4. Visible absorption spectra recorded through Y(010), OP-(10$\bar{1}$), ON(011), and R(111) and a polycrystalline sample of YN.

TABLE 3: Observed and Calculated Wavelengths λ_{max} (nm) and Oscillator Strengths f of the Visible CT Transition in ONA and the Conformers of 1

	observed		ZINDO[a]		TD-DFT[b]		CIS[b]	
molecule	λ_{max}	f	λ_{max}	f	λ_{max}	f	λ_{max}	f
ONA	377[c]	0.11[c]	388[d]	0.19[d]	373[d]	0.09[d]	262[d]	0.25[d]
1[c]	390	0.13	[e]	[e]	[e]	[e]	[e]	[e]
1 (min)[f]	[g]	[g]	378	0.20	351	0.13	243	0.31
1−Y	415	[g]	397	0.20	372	0.13	250	0.34
1−YN	415	[g]	404	0.20	374	0.13	250	0.35
1−ON	419	[g]	415	0.20	420	0.14	263	0.44
1−OP	448	[g]	414	0.19	428	0.15	263	0.43
1−ORP	[g]	[g]	428	0.18	438	0.14	266	0.44
1−R	451	[g]	419	0.16	458	0.14	269	0.42
			453	0.03				

[a] Configuration interaction of all molecular orbitals. [b] Basis set = 6-311+G(2D,P). [c] Cyclohexane solution (10^{-5}M). [d] Calculated using CIS/6-31G(D) optimized structure. [e] Not calculated because multiple conformers coexist in solution. [f] Calculated using HF/6-31G(D) optimized structure. [g] Not measured.

solution (390 nm) and the melt (410 nm). With this offset applied to calculated results, TD-DFT and ZINDO are seen to perform comparably well, both significantly better than CIS.

The calculated ETDMs are shown in the molecular models of the polymorphs in Figure 1 and referenced to individual molecules as "bonds" starting from the phenyl carbon connecting to the nitro group. The ETDMs predicted by different models were parallel to the phenyl ring, as would be expected for a CT transition within the ONA π-system, but differed in their orientations within the phenyl ring. The calculated ETDMs can be compared *in two dimensions* with the observed Amax directions through the crystal sections. The ideal comparison requires that the ETDMs of the molecules in the unit cell project through the crystal section in parallel or antiparallel alignment, as in the cases of Y(010) and R(111) (Figure 1). By symmetry, any Miller plane of the triclinic R and YN ($P\bar{1}$, $Z = 2$) meets this requirement, since the two molecules in the unit cell are inversion-related. However, only the (010) section of the monoclinic Y, ON, and OP ($P2_1/n$ or $P2_1/c$, $Z = 4$) meets this requirement by symmetry.[34]

For Y(010), the ETDM directions predicted by CIS and TD-DFT approximately coincided and matched the observed Amax

direction better than the ZINDO prediction. For R(111), the TD-DFT result and the average of the two ZINDO results approximately coincided and both matched the observed Amax direction better than the CIS result. The double electronic transition of Form R molecules predicted by ZINDO may be a computational anomaly because single transitions were predicted for all other conformers and by other models.

The ETDMs projected through ON(011) deviate slightly from parallel or antiparallel alignment (Figure 1c), making ON(011) less useful for this analysis. Nevertheless, an approximate comparison revealed that TD-DFT and CIS results agree better with the Amax direction than ZINDO. The ETDMs projected through OP($10\bar{1}$) define two directions approximately 40° from each other, making it uninformative for the present analysis.

The foregoing comparisons indicate that TD-DFT performed the best for reproducing observed properties of the visible CT transition of **1** and ONA, followed by ZINDO and then by CIS. Given that a good performance of ZINDO is anticipated from its special calibration on electronic spectra, the performance of TD-DFT should be considered remarkable. This success parallels the success of TD-DFT with rigid small molecules,[25,26] but was demonstrated here with a more complex molecule of low symmetry and conformational flexibility, and using not only λ_{max} and *f* but also the EDTM as criteria. Similar to λ_{max} and *f*, the ETDM direction of a low-symmetry molecule is sensitive to the quality of wave functions and computational theories. Owing to conformational polymorphism, it is possible to "freeze" **1** in six different conformations in van der Waals crystals and excite electronic transitions without causing conformational change (vertical transitions). Spectral properties thus measured are more meaningfully compared with computational results obtained under the assumption of vertical transition using ground-state geometries. These data would be difficult to obtain from gas- or solution-phase studies, wherein multiple conformers are probed simultaneously and conformational change is not hindered upon electronic excitation. The superior performance of TD-DFT, coupled with the ever increasing speed of computers, promises general applications of TD-DFT for first-principle treatment of electronic transitions of complex molecules that otherwise require semiempirical methods.

The satisfactory account of the different crystal spectra by the electronic transitions of isolated molecules and simple medium red-shift indicates that the different crystal colors of **1** ("color polymorphism") arise principally from different molecular conformations. In the language of molecular-orbital theories, the increasing red-shift in the order Y $\approx$ YN < ON < OP < ORP < R originates mainly from the approach to coplanarity of the phenyl and thiophene aromatic rings in the same order, which leads to greater π-conjugation and smaller HOMO/LUMO gap.

It is desirable to examine whether any remaining differences between observed and calculated spectral properties can be traced to the effect of crystal perturbations. With respect to λ_{max}, a possible crystal effect is the large λ_{max} difference observed between polymorphs ON and OP (29 nm) in comparison to that calculated for isolated molecules (+8 nm by TD-DFT and −1 nm by ZINDO; Table 3). Without crystal perturbation, one would expect ON and OP to have similar λ_{max} owing to their similar molecular conformations. Apart from wavelength shifts, crystal effect may modify the polarization or anisotropy of crystal absorption that is defined by simple vector summation of molecular ETDMs (the oriented-gas theory). In the cases of Y(010) and R(111), the discrepancy between the Amax direction and ETDM projections is directly attributable to crystal perturbations. In general cases where ETDM projections through a crystal section are not purely parallel or antiparallel, the crystal effect must be revealed from the polarization ratios and the Amax/Amin directions when the absorption axes are not fixed by crystal symmetry. The treatment of these crystal effects will require the account of excitonic interactions,[35] which for **1** may arise from the moderately strong charge-transfer transition (dipole length 0.7 Å) and the large molecular dipole moments (6−8 D) in the crystalline state. Such an inquiry could be initiated with the present data, but is more suitably postponed until other data are available. For example, it is desirable to acquire higher-resolution crystal spectra at lower temperatures and through other crystal sections (the present data consist of measurements through only one cross section of each polymorph). Single-crystal specular reflection spectroscopy may prove valuable when absorption saturation is significant. Gas-phase spectroscopy may be used to determine the ETDM vector of the free molecule, especially one "frozen" in the ground conformational state by supersonic free-jet expansion or low-temperature matrix isolation.

Conclusions

The crystallization of **1** isolates different conformers, both stable and unstable in solution, into six polymorphs of known crystal structures. This study demonstrates that the color difference between the polymorphs of **1** ("color polymorphism") is well explained by conformational differences, which change the degree of π-conjugation between the *o*-nitroaniline chromophore and the thiophene ring. Observed wavelengths, oscillator strengths, and ETDM directions have been used to compare three computational methods. TD-DFT gave the best reproduction of observed spectral properties, outperforming CIS and even ZINDO. In light of the special calibration of ZINDO on electronic spectra, the performance of TD-DFT should be considered remarkable and parallels its success for predicting electronic spectra of rigid small molecules.

Acknowledgment. The author thanks Prof. Craig J. Eckhardt for valuable discussions.

References and Notes

(1) Byrn, S. R.; Pfeiffer, R. R.; Stowell, J. G. *Solid-State Chemistry of Drugs*, 2nd ed.; SSCI: West Lafayette, IN, 1999.

(2) Yu, L.; Reutzel, S. M.; Stephenson, G. A. *Pharm. Sci. Technol. Today* **1998**, *1*, 118.

(3) Garti, N., Sato, K., Eds. *Crystallization and Polymorphism of Fats and Fatty Acids*; Marcel Dekker: New York, 1988.

(4) Dunitz, J. D.; Bernstein, J. *Acc. Chem. Res.* **1995**, *28*, 193−200. The anti-AIDS drug Norvir presented a dramatic case of a disappearing polymorph [see Health Professional Letter − Abbott (July 28, 1998), http://www.fda.gov/medwatch/safety/1998/norvir.htm]. The original polymorph "disappeared" after a more stable polymorph began to crystallize and Norvir capsules produced with the new polymorph failed the dissolution specification.

(5) Bernstein, J. *J. Phys. D: Appl. Phys.* **1993**, *26*, B67.

(6) Bernstein, J.; Anderson, T. E.; Eckardt, C. J. *J. Am. Chem. Soc.* **1979**, *101*, 541.

(7) Yu, L.; Stephenson, G. A.; Mitchell, C. A.; Bunnell, C. A.; Snorek, S. V.; Bowyer, J. J.; Borchardt, T. B.; Stowell, J. G.; Byrn, S. R.. *J. Am. Chem. Soc.* **2000**, *122*, 585.

(8) Gavezzotti, A.; Fillippini, G. *J. Am. Chem. Soc.* **1995**, *117*, 12299.

(9) Toma, P. H.; Kelly, M. P.; Borchardt, T. B.; Byrn, S. R.; Kahr, B. *Chem. Mater.* **1994**, *6*, 1317.

(10) Jacques, J.; Collet, A.; Wilen, S. H. *Enantiomers, Racemates, and Resolutions*; Krieger Publishing Company: Malabar, Florida, 1991.

(11) Brock, C. P.; Schweizer, W. B.; Dunitz, J. D. *J. Am. Chem. Soc.* **1991**, *113*, 9811−9820.

(12) Yu, L. *J. Pharm. Sci.*, **1995**, *84*, 966.

(13) Staab, E.; Addadi, L.; Leiserowitz, L.; Lahav, M. *Adv. Mater.* **1990**, *2*, 40.

(14) Davey, R. J.; Blagden, N.; Potts, G. D.; Docherty, R. *J. Am. Chem. Soc.* **1997**, *119*, 1767.

(15) Mitchell, C. A.; Yu, L.; Ward, M. D. *J. Am. Chem. Soc.* **2001**, *123*, 10830.

(16) Stephenson, G. A.; Borchardt, T. B.; Byrn, S. R.; Bowyer, J.; Bunnell, C. A.; Snorek, S. V.; Yu, L. *J. Phar. Sci.* **1995**, *84*, 1385.

(17) The Cambridge Crystallographic Data Centre (CCDC), 12 Union Road, Cambridge CB2 1EZ, England.

(18) Despite numerous reports of highly polymorphic systems [see, for example, Kuhnert-Brandstatter, M. *Thermomicroscopy in the Analysis of Pharmaceuticals*; Oxford: Pergamon Press, 1971], systems with many polymorphs *for which crystal structures have been solved at the same temperature* are more rare. Sulfathiazole has five polymorphs of known crystal structures (Hughes, D. S.; Hursthouse, B.; Threlfall, R.; Tavener, S. *Acta Crystallogr.* **1999**, *C55*, 1831).

(19) Bernstein, J. Conformational Polymorphism. In *Organic Solid State Chemistry*; Desiraju, G. R., Ed.; Elsevier: Amsterdam, 1987.

(20) Desiraju, G. R. *Crystal Engineering. The Design of Organic Solids*; Elsevier: Amsterdam, 1989.

(21) Peterson, M. L.; Strnad, J. T.; Markotan, T. P.; Morales, C. A.; Scaltrito, D. V.; Staley, S. W. *J. Org. Chem.* **1999**, *64*, 4(25), 9067.

(22) Yu, L.; Reutzel-Edens, S. M.; Mitchell, C. M. *Org. Process Res. Devel.* **2000**, *4*, 396.

(23) Zerner, M. C.; Loew, G. H.; Kirchner, R. F.; Mueller-Westerhoff, U. T. *J. Am. Chem. Soc.* **1980**, *102*, 589.

(24) Foresman, J. B.; Head-Gordon, M.; Pople, J. A.; Frisch, M. J. *J. Phys. Chem.* **1992**, *96*, 135.

(25) Bauernschmitt, R.; Ahlrichs, R. *Chem. Phys. Lett.* **1996**, *256*, 454.

(26) Casida, M. E.; Jamorski, C.; Casida, K. C.; Salahub, D. R. *J. Chem. Phys.* **1998**, *108*, 4439.

(27) Bernstein, J.; Davey, R. J.; Henck, J.-O. *Angew. Chem., Int. Ed. Engl.* **1999**, *38*, 3441.

(28) Bloss, F. D. *An Introduction to the Methods of Optical Crystallography*; Saunders College Publishing: New York, 1961.

(29) Frisch, M. J.; Trucks, G. W.; Schlegel, H. B.; Scuseria, G. E.; Robb, M. A.; Cheeseman, J. R.; Zakrzewski, V. G.; Montgomery, J. A., Jr.; Stratmann, R. E.; Burant, J. C.; Dapprich, S.; Millam, J. M.; Daniels, A. D.; Kudin, K. N.; Strain, M. C.; Farkas, O.; Tomasi, J.; Barone, V.; Cossi, M.; Cammi, R.; Mennucci, B.; Pomelli, C.; Adamo, C.; Clifford, S.; Ochterski, J.; Petersson, G. A.; Ayala, P. Y.; Cui, Q.; Morokuma, K.; Malick, D. K.; Rabuck, A. D.; Raghavachari, K.; Foresman, J. B.; Cioslowski, J.; Ortiz, J. V.; Stefanov, B. B.; Liu, G.; Liashenko, A.; Piskorz, P.; Komaromi, I.; Gomperts, R.; Martin, R. L.; Fox, D. J.; Keith, T.; Al-Laham, M. A.; Peng, C. Y.; Nanayakkara, A.; Gonzalez, C.; Challacombe, M.; Gill, P. M. W.; Johnson, B. G.; Chen, W.; Wong, M. W.; Andres, J. L.; Head-Gordon, M.; Replogle, E. S.; Pople, J. A. *Gaussian 98*, revision A.9; Gaussian, Inc.: Pittsburgh, PA, 1998.

(30) Becke, A. D. *J. Chem. Phys.* **1993**, *98*, 5648.

(31) The assignment was based on optical-crystallographic theories (see ref 28) and the following evidence: the Kamb angle δ (between extinction and isogyre-disappearance) is 16° (600 nm), ruling out the *zx* section (which requires $\delta < 5°$); the optic sign is (+); the refractive index is greater along the optic axial plane (OAP) than perpendicular to it, indicating CIF = Bx_o (obtuse bisectrix).

(32) Suzuki, H. *Electronic Absorption Spectra and Geometry of Organic Molecules*; Academic Press: New York, 1967.

(33) Oscillator strengths were not determined for crystal sections owing to large errors in the estimation of their thickness and slight absorption saturation observed with OP(101).

(34) To see this conclusion, translate the four ETDM vectors in the unit cell so that their origins coincide at (0, 0, 0). The end points of the ETDMs will now be symmetry-related in the form (x,y,z), $(x,-y,z)$, $(-x,-y,-z)$ and $(-x,y,-z)$. The four ETDM end points define a rectangle. The monoclinic symmetry dictates that the rectangle is perpendicular to (010) and hence the four ETDMs project to a line through (010). Projection of the ETDM rectangle through other Miller planes ordinarily gives a parallelogram and is reduced to a line only by accident.

(35) Craig, D. P. Visible and Ultraviolet Absorption by Molecular Crystals. In *Physics and Chemistry of the Organic Solid State*; Fox, D., Labes, M. M., Weissberger, A., Eds.; Interscience: New York, 1963.